Dual-Stage Adaptive Friction Compensation for Precise Load Side Position Tracking of Indirect Drive Mechanisms

Wenjie Chen, *Member, IEEE*, Kyoungchul Kong, *Member, IEEE*, and Masayoshi Tomizuka, *Fellow, IEEE*

Abstract—This paper investigates the friction compensation of an indirect drive mechanism in the absence of precise end-effector position measurement. Unlike direct drive mechanisms, a typical indirect drive mechanism in the mechanical systems is composed of an actuator (motor side) and an inertia load (load side/end-effector), separated by the gear transmission. Friction in the gear transmission makes the dynamics of the indirect drive mechanism complicated and the precise position control of the end-effector challenging. More specifically, when joint compliance exists in the gear transmission, it is not simple to observe and compensate for the friction. In this paper, a mathematical model and its parameter adaptation method are proposed for the estimation and compensation of the friction in indirect drive mechanisms. For the ultimate objective of tracking the predefined load side reference trajectory, we feed back the estimated friction into the control system by refining the motor side reference trajectory, as well as by adding a feedforward signal to the control input of the motor. Both methods (i.e., the torque compensation and the motor side reference modification) are combined to effectively reject the friction effects in indirect drive mechanisms. The success of the two friction compensation methods depends on their effective integration. For this purpose, a hybrid decision making is adopted to engage or disengage the load side compensation algorithm when the task is repetitive. The proposed method is verified by experimental results on a single-joint indirect drive testbed.

Index Terms—Adaptive observer, friction compensation, hybrid controller, indirect drive, kinematic Kalman filter.

I. INTRODUCTION

INDIRECT drive mechanisms are commonly used in industrial applications because of the high torque capacity. Unlike direct drive mechanisms, a typical indirect drive mechanism in the mechanical systems is composed of an actuator (motor side) and an inertia load (load side/end-effector), separated by the gear transmission. These indirect drive mechanisms may be working by itself alone connecting

W. Chen is with the Robot Laboratory, FANUC Corporation, Oshino-mura 401-0597, Japan (e-mail: wjchen@berkeley.edu).

K. Kong is with the Department of Mechanical Engineering, Sogang University, Seoul 121-742, Korea (e-mail: kckong@sogang.ac.kr).

M. Tomizuka is with the Department of Mechanical Engineering, University of California at Berkeley, Berkeley, CA 94720 USA (e-mail: tomizuka@me.berkeley.edu).

to an end-effector (such as in a machine tool application), or be connected in a serial and/or parallel train as a multi-joint robot manipulator with joint elasticity. In terms of control practice, all these applications share the same fundamental characteristics at the joint level, where the gear transmissions set challenges in high precision motion control because of gear compliances and nonlinearities such as friction and torque hysteresis by backlash. The dynamic modeling of such indirect drive mechanisms (or elastic joint robots) was first introduced in [1] to model the gear compliance as the linear spring element for joint torque transmission. More recent works [2], [3] were performed to demonstrate the nonlinear dynamics in such systems more completely including the friction, hysteresis, and backlash. Because of gear compliances and nonlinearities, the ideal kinematic relationship (e.g., the speed reduction ratio) between the load side (e.g., the link of an elastic joint or an end-effector on a machine tool) and the motor side does not hold. Moreover, since position sensors such as encoders for motion control are normally installed at the motor side for better resolution and easy installation, observation of the actual behavior of the load side is not easy. Particularly, the friction imposed on the load side is difficult to compensate for, because: 1) precise load side position measurement is often unavailable and 2) it is indirectly actuated through the gear transmission. Nevertheless, the load side performance is critical in practical applications, and thus a method that compensates for friction on both the motor side and the load side is necessary.

Over the past several decades, modeling and compensation of the friction effects have been intensively studied from various viewpoints, including static/dynamic characterizations and feedback/feedforward compensation schemes [4]–[7]. For example, many model-based friction compensation techniques have been developed to mitigate the friction effects by adaptively [8] or robustly [9] observing the actual friction. Also, typical approaches, such as the disturbance observer [10] and the repetitive control [11], [12], have been used to compensate for friction.

Most of these studies, however, verified their performance based on simple one-mass systems or direct drives only. When the dynamic characteristics of indirect drive mechanisms, which appear in most industrial mechanical systems, are considered, the friction effects introduced from the load side remain a challenge. Therefore, friction characteristics in harmonic drive systems, one of the representative elastic

transmission mechanisms, were studied in [13] and [14]. The performance and stability issues (e.g., limit cycles) due to friction forces were addressed in [15]. Some compensation schemes were proposed to overcome the friction effects in harmonic drives. Most of them, however, still focused on the motor side compensation only [14], [16]–[18] or torque tracking control [19]. For the tip (load side) trajectory tracking, it has been proposed recently in [20] to use two controllers, where the friction compensator still only considered motor side friction, while the joint flexibility was compensated by a composite controller torque by singular perturbation theory. In those attempts [20]–[22] to enhance the load side performance, the position measurements of both motor side and load side have been used in the controller design. Such controllers, however, are difficult to implement in industrial mechanical systems, which are usually not equipped with sensors for load side position measurement.

In our previous work [23], a friction compensation scheme for the indirect drive mechanism was developed in the absence of position measurement of the load side. The proposed algorithm estimated the friction effects imposed on both the motor side and the load side by a mathematical model and rejected them by two methods, that is, the motor torque manipulation and the motor side reference modification. The successful integration of these two methods relies on the accomplishment of suboptimal motor side performance. This suboptimality can only be determined through some performance measure. For example, such performance measure is possible when the task is repeated, which is common in industrial applications. This scenario was used in [23] and also in this paper to implement the hybrid decision making for the dual-stage friction compensation.

However, the load side position estimation algorithm, which was essential for load side friction compensation, was omitted in [23]. As discussed above, precise load side position measurement (e.g., load side encoder) is usually not available in industrial applications because of cost and assembly issues. To overcome this problem, the inexpensive MEMS (microelectro-mechanical systems) sensors such as an inertia measurement unit (IMU)[1] that are easy to mount may be considered. Consideration should be given, however, to problems such as nonnegligible biases, limited bandwidth, and noises from low-cost sensors, which set restrictions on the direct usage of sensor signals. As shown in [25], these problems may be circumvented by the proper fusion of multiple sensor signals, such as the signals from the motor encoder and the load side MEMS gyroscope and accelerometer.

In this paper, the dual-stage friction compensation scheme in [23] is reviewed with more complete details. The sensor fusion algorithm by fusing motor encoder and load side MEMS inertia sensor measurements is formulated for load side position estimation and friction compensation. The two compensation stages (i.e., torque compensation and motor side reference modification) are properly combined using a hybrid system structure for effective compensation of the
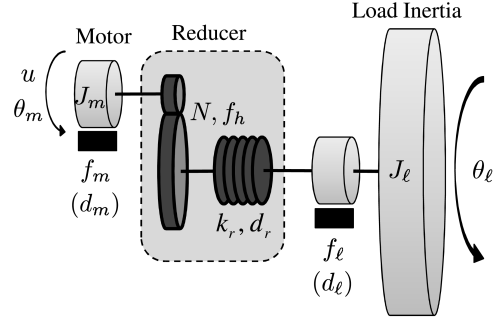
---

[1]A representative cost comparison between the encoders and the MEMS inertia sensors can be found in [24].

Fig. 1. Single-joint indirect drive mechanism.

friction effects. The effectiveness of the proposed method is verified by experimental results.

II. SYSTEM OVERVIEW

A. Single-Joint Indirect Drive Model

Instead of the sophisticated complete dynamic models proposed in [2] and [3], this paper uses a simpler dynamic model, which is more tractable for control purpose, with a focus on the nonlinear friction compensation. Also different from [1], the gear compliance is modeled as a linear spring and a linear damping here to capture more subtle joint torque transmission dynamics. Fig. 1 shows the schematic of a single-joint indirect drive mechanism. The subscripts m and ℓ denote the motor side and the load side quantities, respectively. d represents the viscous damping coefficient, and J is the moment of inertia. θ and u represent the angular position and motor torque output, respectively. k_r and d_r are the stiffness and the damping coefficients of the gear reducer. The gear ratio of the reducer is denoted by N. f_m, f_ℓ, and f_h represent the nonlinear friction forces at the motor side, the load side, and the reducer, respectively. Note that f_m and f_ℓ include the viscous damping effects d_m and d_ℓ, respectively. These friction forces are further discussed later.

Equations of motion for the system in Fig. 1 are

$$J_m\ddot{\theta}_m + f_m + f_h = u - \frac{1}{N}\left[k_r\left(\frac{\theta_m}{N} - \theta_\ell\right) + d_r\left(\frac{\dot{\theta}_m}{N} - \dot{\theta}_\ell\right)\right]$$
(1)

$$J_\ell\ddot{\theta}_\ell + f_\ell = k_r\left(\frac{\theta_m}{N} - \theta_\ell\right) + d_r\left(\frac{\dot{\theta}_m}{N} - \dot{\theta}_\ell\right).$$
(2)

B. Friction Model

In the system shown in Fig. 1, the energy is dissipated mainly by three friction forces: 1) the motor (wave generator) bearing friction, f_m; 2) the load output bearing friction, f_ℓ; and 3) the gear meshing friction, f_h. Although the gear meshing friction f_h is dominant in a free load condition [13], the load side friction f_ℓ can become more significant as the load side inertia increases. Note that, both the motor side friction f_m and the gear meshing friction f_h are functions of the motor side velocity $\dot{\theta}_m$, while the load side friction f_ℓ is a function of the load side velocity $\dot{\theta}_\ell$ [13].

The combination of system model (1)–(2) gives

$$J_m \ddot{\theta}_m + \frac{1}{N} J_\ell \ddot{\theta}_\ell = u - F \qquad (3)$$

where $F = f_m + f_h + f_\ell / N$ can be explained as the entire friction force imposed on the whole system referred to the motor side.

There are several reasons to model the entire friction force F as reflected on the motor side. First of all, it is very difficult and often impossible to identify these frictions separately at their actual different locations (i.e., motor side, gear, and load side). It is, however, easier to identify the friction entirely on the motor side for transmission systems. Second, from the torque compensation point of view, the friction force is usually compensated at the motor side where the actuator is. Therefore, we propose a compromised way to group all the friction forces together as an entire friction F for modeling and estimation. This is based on the fact that these friction forces often exhibit similar behaviors, especially for the motion periods without velocity reversals.

It is, however, noted that no generic friction models can still strictly capture the characteristics of the grouped entire friction F. In this case, we use Lund–Grenoble (LuGre) model [5] for its ability to capture more dynamic behaviors and that it has more parameters than the static friction models, thus providing more degrees of freedom to fit with the entire friction characteristics. The LuGre model uses an internal friction state, z, governed by

$$\dot{z} = v - \frac{\beta_0 |v|}{g(v)} z \qquad (4)$$

$$g(v) = F_c + (F_s - F_c) e^{\left(-v^2/v_s^2\right)} \qquad (5)$$

$$F = \sigma_0 z + \sigma_1 \dot{z} + \sigma_2 v \qquad (6)$$

where v is the relative velocity between the two contacting surfaces at the motor side, that is, $v = \dot{\theta}_m$. σ_0, σ_1, and σ_2 represent the microstiffness, microdamping of the internal state z, and the macrodamping of the velocity v, respectively. The function $g(v)$ is chosen to capture the Stribeck effect, where F_C and F_S are the levels of Coulomb friction and stiction force, respectively. v_s is the Stribeck velocity, and the exponential shape parameter of the Stribeck effect is set as 2, which follows the common practice in the standard LuGre model [5], [8]. The internal friction state z can be regarded as the deflection of bristles, which represents the asperities between the two contacting surfaces.

In (4), note that an additional parameter, β_0, is used to define the nominal microstiffness of the internal state z, which differs from the standard LuGre model. This modification will simplify the adaptive friction compensation algorithm.

Equations (4)–(6) give the entire friction force, F, as

$$F = K^T \Phi \qquad (7)$$

where $K = [\sigma_1 + \sigma_2, \ \sigma_0, \ \beta_0 \sigma_1]^T$, $\Phi = [v, \ z, \ -|v|/g(v)z]^T$.

Notice that the modified LuGre model still preserves the following property of standard LuGre model [5].

Property 1: $F_c \leq g(v) \leq F_s$. $|z(t)| \leq F_s/\beta_0$, $\forall t \geq 0$ if $|z(0)| \leq F_s/\beta_0$.

Proof: It is easy to see from (5) that $F_c \leq g(v) \leq F_s$. Therefore, if $z = F_s/\beta_0$, then $\beta_0 |v|/g(v)z \geq |v|$, which leads to $\dot{z} = v - \beta_0 |v|/g(v)z \leq 0$. Similarly, $z = -F_s/\beta_0$ leads to $\dot{z} = v - \beta_0 |v|/g(v)z \geq 0$. Thus, as long as z starts from $|z(0)| \leq F_s/\beta_0$, we have $|z(t)| \leq F_s/\beta_0$, $\forall t \geq 0$. ∎

Remark 1: Assume the system starts from rest when powering up, that is, $\ddot{\theta}_m(t \leq 0) = \ddot{\theta}_\ell(t \leq 0) = 0$ and $u(t \leq 0) = 0$. Then the dynamic model (3) leads to $F(t \leq 0) = 0$. From the friction model (4)–(6),[2] we can conclude that $z(t \leq 0) \rightarrow 0$, which satisfies $|z(0)| \leq F_s/\beta_0$. Therefore, $|z(t)| \leq F_s/\beta_0$, $\forall t \geq 0$. This property will be used in the subsequent controller design to ensure the bounded stability of the friction observer.

Remark 2: In practice, friction characteristics may vary because of the variations of the normal force in contact, lubricant condition, temperature, material wear, and so on [8]. Variations in the normal force usually cause an impact only on the static parameters, that is, F_C, F_S, v_s, and σ_2, while the changes in lubricant condition, temperature, and/or materials may affect both static and dynamic parameters.

Remark 3: If only static friction is considered, that is, $\dot{z} = 0$, the modified LuGre model is reduced to

$$F(v) = \frac{\sigma_0}{\beta_0} \left[F_c + (F_s - F_c) e^{\left(-v^2/v_s^2\right)} \right] \ \mathrm{sgn}(v) + \sigma_2 v. \qquad (8)$$

This indicates that, by fixing the nominal microstiffness, β_0, the adaptation of real microstiffness, σ_0, effectively changes the level of static parameters, for example, F_C and F_S in $g(v)$. Thus, the adaptation of σ_0, σ_1, and σ_2 can account for most parameter variations in the modified friction model regardless of the dynamics for internal state z. Accordingly, K in (7), which consists of σ_0, σ_1, and σ_2, is chosen to be adapted in real-time with Φ as the regressor.

In the case that the load side friction effects are not negligible, it is necessary to consider the load side friction separately. Assuming that the load side friction shares the similar characteristics as the entire friction force, F, a ratio r_ℓ can be introduced to derive the load side friction f_ℓ from F, that is

$$f_\ell = r_\ell F. \qquad (9)$$

This assumption is reasonable in most cases, especially when the motor is spinning in one direction.[3] The transient behavior during the velocity reversal may not strictly follow the assumption. This velocity reversal case, however, is not of major interest in most mid-to-high-speed applications since the transient time is usually sufficiently short (to be negligible).

---

[2] $F(t \leq 0) = 0$, $v(t \leq 0) = \dot{\theta}_m(t \leq 0) = 0 \Longrightarrow \dot{z}(t \leq 0) = -\sigma_0/\sigma_1 z(t \leq 0) \Longrightarrow z(t \leq 0) \rightarrow 0$.

[3] For one directional spinning or mid-to-high-speed applications, the "traditional" friction compensation is normally not a problem since the feedback controller may be able to compensate for the Coulomb friction and viscous damping at the steady state. This in fact corresponds to the motor side friction compensation introduced later. However, as shown later in the experiments, this load side friction causes the offset in the load side position tracking error, which cannot be removed by the feedback controller (with motor side friction compensation) only, even in the one-directional spinning or mid-to-high-speed applications. Therefore, the load side friction compensation is still necessary in a nontraditional sense by modifying the motor side reference trajectory in such applications, where this load side friction modeling is mostly valid.
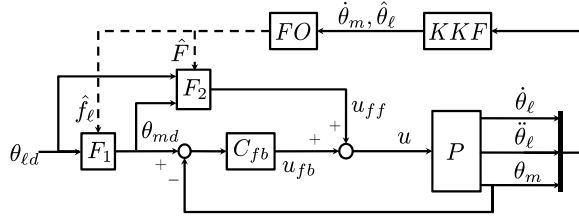
Fig. 2. Block diagram of the overall control system.

C. Controller Structure

Fig. 2 shows the overall control structure of the single-joint indirect drive mechanism, where P denotes the system plant with the measurable outputs as the motor side position θ_m, load side velocity $\dot{\theta}_\ell$, and load side acceleration $\ddot{\theta}_\ell$ (i.e., assume that the system is equipped with motor encoder, load side gyroscope, and load side accelerometer). The proposed control structure has two nested loops. The inner loop (i.e., feedforward controller F_2 and feedback controller C_{fb}) uses the motor torque u as the control to the plant to achieve motor side tracking, which is the common practice in industrial applications. The joint flexibility of the indirect drive mechanism is addressed in the outer loop (i.e., feedforward controller F_1), which uses the motor side reference θ_{md} as the control to the inner loop to achieve the ultimate objective, that is, load side tracking. Additionally, the state estimator, kinematic Kalman filter (KKF), and the friction observer, FO, are constructed in the following sections to provide necessary estimates for control use.

Here the state estimator KKF denotes the kinematic Kalman filter method to estimate the load side position θ_ℓ, while the friction observer FO adaptively estimates the entire friction F and the load side friction f_ℓ to be used in the feedforward controllers F_2 and F_1. The feedforward controller, F_2, is designed from (3) as

$$u_{ff}(t) = J_m \ddot{\theta}_{md}(t) + \frac{1}{N} J_\ell \ddot{\theta}_{\ell d}(t) + \hat{F}(t) \tag{10}$$

where $\hat{F}$ is the estimated entire friction force. $\ddot{\theta}_{\ell d}$ is the desired load side acceleration. In the case where the acceleration is measured by a sensor (e.g., load side accelerometer), $\ddot{\theta}_{\ell d}$ can be replaced with $\ddot{\theta}_\ell$. θ_{md} is the motor side position reference generated by F_1 from the desired load side position, $\theta_{\ell d}$, that is

$$\theta_{md}(t) = \frac{N}{k_r}[J_\ell \ddot{\theta}_{\ell d}(t) + \hat{f}_\ell(t)] + N\theta_{\ell d}(t) \tag{11}$$

where $\hat{f}_\ell$ is the estimated load side friction. Equation (11) is derived from (2) by neglecting the joint damping d_r, since $k_r (\theta_m/N - \theta_\ell) \gg d_r (\dot{\theta}_m/N - \dot{\theta}_\ell)$ usually holds within the system bandwidth. Note that (11) provides a control degree of freedom by modifying the motor side reference trajectory θ_{md}, while the desired load side reference trajectory $\theta_{\ell d}$ is often predefined and fixed for the real-time control practice.

The feedback controller, C_{fb}, is a modified PID controller described as

$$C_{fb}(s) = \left(k_v + \frac{k_i}{s}\right)(s + k_p) \tag{12}$$

where k_p is the proportional gain of the position loop, k_v and k_i are the proportional-integral (PI) gains of the velocity loop. s is the complex variable in the Laplace domain. Note that s in the second parentheses is to generate the velocity error for the velocity loop. The above controller is discretized by the Euler method for implementation.

III. FRICTION COMPENSATION

As shown in the controller structure (10)–(11), the proposed friction compensator consists of two parts. The motor side friction compensation is designed in the feedforward controller F_2 by injecting the torque input as in (10), and the load side friction effects are further compensated in the feedforward controller F_1 by manipulating the motor side reference, θ_{md}, as in (11).

A. Motor Side Friction Compensation

1) Feedback Friction Compensation: Let $e_m = \theta_m - \theta_{md}$ be the motor side position tracking error. Define a first-order sliding surface, p_m, as

$$p_m = \dot{e}_m + k_s e_m \tag{13}$$

where k_s is a positive constant. Note that e_m is small or converges to zero if p_m is small or converges to zero, since $e_m(s)/p_m(s) = 1/(s + k_s)$ is asymptotically stable.

From (3) and (13), the motor side error dynamics is derived as

$$J_m \dot{p}_m = u - F - \frac{1}{N} J_\ell \ddot{\theta}_\ell - J_m \ddot{\theta}_{md} + J_m k_s \dot{e}_m. \tag{14}$$

The controller structure yields the following control law:

$$\begin{aligned} u(t) &= u_{ff}(t) + u_{fb}(t) \\ &= \left[J_m \ddot{\theta}_{md}(t) + \frac{1}{N} J_\ell \ddot{\theta}_{\ell d}(t) + \hat{F}(t)\right] \\ &\quad - \left[k_v s_m(t) + \int_0^t k_i s_m(\tau)d\tau\right] \end{aligned} \tag{15}$$

where $s_m(t) = \dot{e}_m(t) + k_p e_m(t)$ is the error term in the velocity loop.

By applying the adaptive control technique, an adaptive friction observer is designed to obtain $\hat{F}(t)$ as

$$\hat{F} = \hat{K}^{\mathrm{T}} \hat{\Phi} \tag{16}$$

where $\hat{\Phi} = [\dot{\theta}_m, \ \hat{z}_0, \ -|\dot{\theta}_m|/g(\dot{\theta}_m)\hat{z}_1]^{\mathrm{T}}$. $\hat{K}$, $\hat{z}_0$, and $\hat{z}_1$ are the estimates obtained from the following update laws:

$$\dot{\hat{K}} = -\Gamma \hat{\Phi} p_m \tag{17}$$

$$\dot{\hat{z}}_0 = \dot{\theta}_m - \frac{\beta_0 |\dot{\theta}_m|}{g(\dot{\theta}_m)} \hat{z}_0 - \gamma_3 p_m \tag{18}$$

$$\dot{\hat{z}}_1 = \dot{\theta}_m - \frac{\beta_0 |\dot{\theta}_m|}{g(\dot{\theta}_m)} \hat{z}_1 + \gamma_4 \frac{|\dot{\theta}_m|}{g(\dot{\theta}_m)} p_m \tag{19}$$

where $\Gamma = \mathrm{diag}(\gamma_0, \gamma_1, \gamma_2)$, γ_3 and γ_4 are positive adaptation gains. Notice that the unmeasurable internal friction state z is estimated by a dual-observer structure [26] with two state

estimates, $\hat{z}_0$ and $\hat{z}_1$. Equations (18) and (19) result in the following observer error dynamics:

$$\dot{\tilde{z}}_0 = -\frac{\beta_0 |\dot{\theta}_m|}{g(\dot{\theta}_m)}\tilde{z}_0 + \gamma_3 p_m \qquad (20)$$

$$\dot{\tilde{z}}_1 = -\frac{\beta_0 |\dot{\theta}_m|}{g(\dot{\theta}_m)}\tilde{z}_1 - \gamma_4 \frac{|\dot{\theta}_m|}{g(\dot{\theta}_m)} p_m \qquad (21)$$

where $\tilde{z}_0 = z - \hat{z}_0$ and $\tilde{z}_1 = z - \hat{z}_1$ are the estimation errors of the same internal state z.

2) Stability Analysis: The following theorem proves the stability of the closed-loop system under additional assumptions as stated therein.

Theorem 1: For the system model described by (1)–(6), global asymptotic tracking performance on the motor side can be achieved by the proposed controller in (10)–(12) and the adaptive friction observer in (16)–(19), if the integrator term of the feedback controller, C_{fb}, is suppressed, that is, $k_i = 0$, and the real load side acceleration measurement, $\ddot{\theta}_\ell$, is used in (10).

Proof: Suppose that the feedback controller gains are

$$k_p = \frac{hk_s}{J_m k_s + h}, \quad k_v = J_m k_s + h \qquad (22)$$

where h is a positive constant. By the assumption in the theorem, $k_i = 0$. Then the control law in (15) reduces to

$$u = \left(J_m \ddot{\theta}_{md} + \frac{1}{N} J_\ell \ddot{\theta}_{\ell d} + \hat{F} \right) - (J_m k_s \dot{e}_m + h p_m). \quad (23)$$

From (14) and (23), the control law results in the following closed loop dynamics:

$$J_m \dot{p}_m = -h p_m - \frac{J_\ell}{N}(\ddot{\theta}_\ell - \ddot{\theta}_{\ell d}) - (F - \hat{F})$$

$$= -h p_m - \frac{J_\ell}{N}\ddot{\tilde{e}}_\ell - \tilde{K}^{\mathrm{T}}\hat{\Phi} - K^{\mathrm{T}}\tilde{\Phi} \qquad (24)$$

where $\ddot{\tilde{e}}_\ell = \ddot{\theta}_\ell - \ddot{\theta}_{\ell d}$ is the load side acceleration tracking error, $\tilde{K} = K - \hat{K}$ and $\tilde{\Phi} = \Phi - \hat{\Phi}$ are the estimation errors.

Let a Lyapunov function candidate for the system be

$$V = \frac{1}{2}J_m p_m^2 + \frac{1}{2}\tilde{K}^{\mathrm{T}}\mathrm{diag}(\gamma_0, \gamma_1, \gamma_2)^{-1}\tilde{K} + \frac{1}{2\gamma_3}k_1 \tilde{z}_0^2$$

$$+ \frac{1}{2\gamma_4}k_2 \tilde{z}_1^2 \qquad (25)$$

where $k_1 = \sigma_0$ and $k_2 = \beta_0\sigma_1$ are the last two entries in K.

In most applications, it is reasonable to assume that the actual friction parameters, $K = [\sigma_1 + \sigma_2, \ \sigma_0, \ \beta_0\sigma_1]^{\mathrm{T}}$, are unknown but constant. It follows that $\dot{K} = \mathbf{0}$ and $\dot{\tilde{K}} = -\dot{\hat{K}}$. Therefore, differentiating V in (25) and substituting the update laws from (17)–(19), the derivative of V is obtained as

$$\dot{V} = -h p_m^2 - \frac{J_\ell}{N} p_m \ddot{\tilde{e}}_\ell - \frac{k_1}{\gamma_3}\frac{\beta_0 |\dot{\theta}_m|}{g(\dot{\theta}_m)}\tilde{z}_0^2 - \frac{k_2}{\gamma_4}\frac{\beta_0 |\dot{\theta}_m|}{g(\dot{\theta}_m)}\tilde{z}_1^2. \qquad (26)$$

Recall that h is a positive constant. Thus, every term on the right hand side of (26), except for the second term, is negative semidefinite. Moreover, if the load side acceleration

is measured by sensors (i.e., $\ddot{\theta}_{\ell d}$ is replaced with $\ddot{\theta}_\ell$ in u_{ff} in (10)), the second term becomes zero. It follows that:

$$\dot{V} = -h p_m^2 - \frac{k_1}{\gamma_3}\frac{\beta_0 |\dot{\theta}_m|}{g(\dot{\theta}_m)}\tilde{z}_0^2 - \frac{k_2}{\gamma_4}\frac{\beta_0 |\dot{\theta}_m|}{g(\dot{\theta}_m)}\tilde{z}_1^2 \le -h p_m^2. \qquad (27)$$

From Lyapunov stability theory [27], it is concluded that the motor side tracking error, p_m, the friction parameter estimation error, $\tilde{K}$, and the internal friction state estimation errors, $\tilde{z}_0$ and $\tilde{z}_1$, are globally uniformly bounded. Since the actual friction parameters K are assumed to be constant during one trajectory task, and actual internal friction state, z, is bounded as shown in Property 1, it follows that the estimates, $\hat{K}$, $\hat{z}_0$, and $\hat{z}_1$, are globally uniformly bounded as well. In addition, the actual motor side position and velocity, θ_m and $\dot{\theta}_m$, are globally uniformly bounded, since p_m is globally uniformly bounded, and the generated motor side reference θ_{md} is bounded by the characteristics of the feedforward controller, F_1. With all these bounded variables, it can be shown that $\ddot{V}$ is also bounded. Then by Barbalat's lemma, (25) and (27) imply that $\dot{V} \to 0$ (i.e., $p_m \to 0$) as $t \to \infty$. Therefore, the motor side tracking error $e_m = 1/(s + k_s)p_m$ asymptotically converges to zero. ■

Remark 4: The proposed motor side friction compensation is in a framework of model reference adaptive control [27], [28]. The foregoing theorem shows that this scheme can achieve the asymptotic motor side tracking performance while the parameter estimation errors are globally uniformly bounded. In practice, we often do not need accurate parameter identification which requires the trajectory to be persistently exciting. Instead, we are mainly interested in reducing the tracking error for any general trajectory including the uniform periodic trajectory used later for experiments.

Remark 5: The preceding theorem provides a sufficient condition to achieve global asymptotic tracking performance on the motor side. Two assumptions were introduced to theoretically guarantee the stability of the proposed method. These assumptions, however, may be relaxed without jeopardizing the closed loop stability of the system in practice. The relaxation is demonstrated in the experiments with preserved integrator in C_{fb} to maintain the basic feedback controller structure (i.e., $k_i \ne 0$). Also, the desired reference $\ddot{\theta}_{\ell d}$ is used in (10) instead of the real measurement $\ddot{\theta}_\ell$ to decrease the dependence on the load side sensors.

3) Feedforward Friction Compensation: The above friction compensation scheme is in the feedback form, since the actual physical measurements are used in the regressor estimate, $\hat{\Phi}$. When doing tracking control, feedforward control often improves the performance in the sense that it allows anticausal terms in the controller. It recovers the limitation of feedback controller due to the dynamic lag of the plant [6]. Recall that the feedback controller must see an error first before it can take any corrective action. In particular, this limitation affects the performance during the quick direction reversals of Coulomb friction force.

By replacing the measurements in the friction observer regressor $\hat{\Phi}$ with corresponding trajectory references, and excluding the motor side error term, p_m, a feedforward version

of the regressor, $\hat{\Phi}_d$, is obtained as

$$\hat{\Phi}_d = \left[\dot{\theta}_{md}, \; \hat{z}_d, \; -\frac{|\dot{\theta}_{md}|}{g(\dot{\theta}_{md})}\hat{z}_d\right]^{\mathrm{T}} \tag{28}$$

$$\dot{\hat{z}}_d = \dot{\theta}_{md} - \frac{\beta_0|\dot{\theta}_{md}|}{g(\dot{\theta}_{md})}\hat{z}_d. \tag{29}$$

In this form, the dual estimations of internal friction state z are replaced by single desired (nominal) internal state $\hat{z}_d$ as in (29). Furthermore, the friction observer structure is simplified by reducing the number of adaptive variables from 5 to 3, and the noises and disturbances from feedback measurements are also avoided.

B. Load Side Friction Compensation

Because of the characteristics of indirect drive mechanisms, perfect tracking performance on the motor side does not guarantee perfect load side tracking performance. Since the load side performance is of most interest in practical applications, friction compensation should also be considered on the load side in the way of modifying motor side reference trajectory as in (11), where the load side friction f_ℓ is adaptively estimated as follows.

In (9), the load side friction, f_ℓ, is modeled as a scaled quantity of the entire friction force, F. Thus, once friction parameters are adapted successfully on the motor side, the load side friction f_ℓ can be estimated as

$$\hat{f}_\ell = \hat{r}_\ell \hat{F} \tag{30}$$

where $\hat{F}$ is the estimated entire friction force from the motor side friction compensator and $\hat{r}_\ell$ is the estimated scaling factor obtained by the following update laws:

$$\dot{\hat{r}}_\ell = -\gamma_{r_\ell}\hat{F}\hat{e}_\ell, \quad \hat{e}_\ell = \hat{\theta}_\ell - \theta_{\ell d} \tag{31}$$

where $\gamma_{r_\ell} > 0$ is the adaptation gain and $\hat{\theta}_\ell$ is the load side position estimated by the KKF scheme detailed later.

Remark 6: The adaptation law (31) is an *ad hoc* controller law. The mathematical derivation and stability proof rely on many assumptions to help simply the problem and thus are of little significance. However, the intuition behind this *ad hoc* law can be easily conveyed. From (30) to (31), we can get the time derivative of the load side friction estimate as

$$\dot{\hat{f}}_\ell(\tau) = \dot{\hat{r}}_\ell(\tau)\hat{F}(\tau) + \hat{r}_\ell(\tau)\dot{\hat{F}}(\tau)$$
$$= -\gamma_{r_\ell}\hat{F}^2(\tau)\hat{e}_\ell(\tau) + \left(\hat{r}_\ell(0) - \int_0^\tau \gamma_{r_\ell}\hat{F}(\epsilon)\hat{e}_\ell(\epsilon)d\epsilon\right)\dot{\hat{F}}(\tau). \tag{32}$$

Thus, by integration, the load side friction estimate becomes

$$\hat{f}_\ell(t) = \hat{f}_\ell(0) + \int_0^t \dot{\hat{f}}_\ell(\tau)d\tau$$
$$= \hat{f}_\ell(0) + \int_0^t \left[-\gamma_{r_\ell}\hat{F}^2(\tau)\hat{e}_\ell(\tau)\right.$$
$$\left. + \left(\hat{r}_\ell(0) - \int_0^\tau \gamma_{r_\ell}\hat{F}(\epsilon)\hat{e}_\ell(\epsilon)d\epsilon\right)\dot{\hat{F}}(\tau)\right]d\tau \tag{33}$$

where $\hat{e}_\ell = \hat{\theta}_\ell - \theta_{\ell d}$ is the estimated load side position tracking error. This friction estimate (33) is fed back as in (11) into
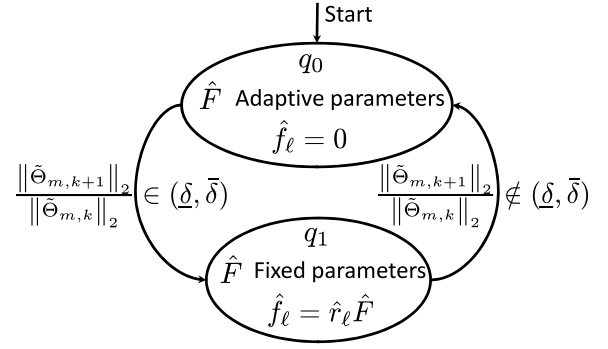

Fig. 3. Hybrid compensator structure.

the motor side reference θ_{md}, which serves as the control of the outer loop for load side tracking. Therefore, this load side friction compensation becomes essentially an integral feedback of load side tracking error $\hat{e}_\ell$.

Remark 7: As seen from (11), the joint stiffness k_r may affect the load side friction compensation. In practice, this stiffness constant is normally given in the reducer specification, and can also be identified through system identification.

Even if this stiffness constant is not accurately known to the controller, the proposed compensator mechanism is still able to effectively improve load side tracking through the adaptive estimate of the load side friction. As it is shown above that the load side friction compensation is essentially an integral feedback of load side position error $\hat{e}_\ell$, the joint stiffness constant k_r will affect such feedback performance as a part of the integral gain. This effect, however, can be offset by the tuning of the adaptation gain γ_{r_ℓ}.

C. Hybrid Compensator Structure

Note that in (11), the load side friction estimate, $\hat{f}_\ell$, is injected into the motor side reference, θ_{md}. Thus, it is desired that the compensated reference is still smooth and differentiable, since the motor side velocity reference, $\dot{\theta}_{md}$, is needed in the feedback controller, C_{fb}. To ensure this, the load side compensation should be activated only when the friction parameters in the motor side compensator have converged to some suboptimal values and then set fixed [i.e., $\Gamma = \mathbf{0}$, which means the adaptation law (17) is disabled].

As discussed in the introduction, the convergence of motor side compensation performance can only be checked by some performance measure. Such performance measure is possible in industrial applications, where the same task is usually executed repeatedly. Define $\|\tilde{\Theta}_{m,k}\|_2$ as the two-norm of the motor side position tracking error in the kth execution of the same task, that is

$$\|\tilde{\Theta}_{m,k}\|_2 = \left(\sum_{i=1}^n |\theta_{m,k}(i) - \theta_{md}(i)|^2\right)^{\frac{1}{2}} \tag{34}$$

where i is the time index and n defines the duration of each execution.

Therefore, the above compensation activation logic can be formalized by the hybrid compensator structure shown in Fig. 3. q_0 and q_1 are the two discrete controller states. The

controller starts from the state q_0, where the adaptive motor side compensator is activated, and the load side compensator is disabled (i.e., $\hat{f}_\ell = 0$).

If $\|\tilde{\Theta}_{m,k+1}\|_2 / \|\tilde{\Theta}_{m,k}\|_2 \in (\underline{\delta}, \bar{\delta})$, where $(\underline{\delta}, \bar{\delta})$ is the convergence boundary (e.g., $\underline{\delta}$ and $\bar{\delta}$ are positive numbers very close to 1), the compensator scheme is switched to the state q_1. This means that the friction adaptation in the motor side compensator has reached its suboptimal stage, and cannot significantly improve the motor side tracking performance. At this stage q_1, the load side compensator is enabled while the friction parameters in the motor side compensator are fixed (i.e., $\Gamma = \mathbf{0}$).

If $\|\tilde{\Theta}_{m,k+1}\|_2 / \|\tilde{\Theta}_{m,k}\|_2 \notin (\underline{\delta}, \bar{\delta})$, this indicates that the motor side tracking performance can be further improved by adapting the parameters in the motor side compensator. Thus, the compensator scheme is switched back to the initial state q_0.

Remark 8: Note that although our ultimate objective is to enhance the load side tracking performance by friction compensation, the motor side friction compensation is still necessary and of significance for two reasons. First of all, as seen from friction modeling, the load side friction is approximated as a proportional term of the entire friction, which can be identified more easily from the motor side with more sensing information available. Secondly, as seen from (10), once this entire friction is estimated, it can be readily compensated for from the motor side where the actuator is. The motor side compensation performance in turn provides a metric to check whether the friction estimation is ready for the load side friction compensation (as seen from the hybrid compensator structure). Therefore, the load side friction compensation, which is related to our ultimate objective, is greatly relying on the success of motor side friction compensation.

IV. KINEMATIC KALMAN FILTER

Note that the load side position information is essential in the load side friction estimation and compensation (30)–(31). This section presents the KKF to estimate the load side position by fusing the signals from the available motor encoder and economic load side MEMS gyroscope and accelerometer.

A. Model for Measurement Dynamics

The bias and the noise in the sensor output are described as

$$\dot{b}(t) = n_b(t) \tag{35a}$$
$$y_s(t) = y(t) + b(t) + n_s(t) \tag{35b}$$

where b is the bias of the sensor output varying with the fictitious noise n_b and y_s is the sensor measurement for the actual physical quantity y with the measurement noise n_s.

B. System Kinematic Model

The kinematic model from the acceleration to the position on the load side can be written as

$$\frac{d}{dt} \begin{bmatrix} \theta_\ell(t) \\ \dot{\theta}_\ell(t) \end{bmatrix} = \begin{bmatrix} 0 & 1 \\ 0 & 0 \end{bmatrix} \begin{bmatrix} \theta_\ell(t) \\ \dot{\theta}_\ell(t) \end{bmatrix} + \begin{bmatrix} 0 \\ 1 \end{bmatrix} \ddot{\theta}_\ell(t). \tag{36}$$

The Kalman filter based on the kinematic model (36) is called the KKF [29]. In KKF, the acceleration is used as an input to the filter, and the position measurement is used to correct the estimation output.

Here, an original but intuitive method is proposed to approximate the load side position measurement. Let $G_{m2l}(s)$ be the transfer function from the motor side position θ_m to the load side position θ_ℓ, that is

$$G_{m2l}(s) \triangleq \frac{\theta_\ell(s)}{\theta_m(s)} = \frac{d_r s + k_r}{N[J_\ell s^2 + (d_r + d_\ell)s + k_r]} \tag{37}$$

by the inherent system dynamics (1)–(2). Thus, $G_{m2l}(s)$ is approximately zero-phase static gain at the low-frequency region, since the dynamic chain from θ_m to θ_ℓ is modeled by mass, gear, spring, and damper. Therefore, the low-frequency component of θ_ℓ can be approximated by that of θ_m.

Pass θ_m and θ_ℓ through a first-order low-pass filter $G_f(s) = \alpha/(s + \alpha)$, where α is the filter bandwidth to be designed. Denote the filter outputs as θ_{mf} and $\theta_{\ell f}$, respectively. It follows that:

$$\dot{\theta}_{mf} = -\alpha\theta_{mf} + \alpha\theta_m \tag{38a}$$
$$\dot{\theta}_{\ell f} = -\alpha\theta_{\ell f} + \alpha\theta_\ell. \tag{38b}$$

The above analysis shows that, if α is chosen properly (e.g., less than the bandwidth of $G_{m2l}(s)$), the filter outputs will have the following relation:

$$\theta_{\ell f} \approx \frac{1}{N}\theta_{mf}. \tag{39}$$

The filter dynamics (38) and the measurement dynamics (35) can be added into the system kinematic model (36), giving

$$\dot{x}_k(t) = \mathbf{A}_k x_k(t) + \mathbf{B}_{k,u}\ddot{\theta}_{\ell,s}(t) + \mathbf{B}_{k,w}w_k(t) \tag{40a}$$
$$y_k(t) = \mathbf{C}_k x_k(t) + v_k(t) \tag{40b}$$

where

$$x_k = [\theta_{\ell f} \quad \theta_\ell \quad \dot{\theta}_\ell \quad -b_a \quad b_v]^{\mathrm{T}}$$
$$y_k = [\theta_{\ell f,s} \quad \dot{\theta}_{\ell,s}]^{\mathrm{T}}$$
$$w_k = [-n_{a\ell} \quad -n_{ba} \quad n_{bv}]^{\mathrm{T}}$$
$$v_k = [n_{\ell f} \quad n_{v\ell}]^{\mathrm{T}}$$
$$\mathbf{A}_k = \begin{bmatrix} -\alpha & \alpha & 0 & 0 \\ 0 & 0 & 1 & 0 & \mathbf{0} \\ 0 & 0 & 0 & 1 \\ \hline & \mathbf{0} & & & \mathbf{0} \end{bmatrix}$$
$$\mathbf{B}_{k,u} = [0 \quad 0 \quad 1 \quad 0 \quad 0]^{\mathrm{T}}$$
$$\mathbf{B}_{k,w} = [\mathbf{0} \mid I_3]^{\mathrm{T}}$$
$$\mathbf{C}_k = \begin{bmatrix} 1 & 0 & 0 & 0 & 0 \\ 0 & 0 & 1 & 0 & 1 \end{bmatrix}$$

where the subscripts a and v indicate the load side accelerometer and gyroscope quantities, respectively. $\bullet_s$ is the sensor measurement of the actual quantity $\bullet$, $b_\bullet$ is the bias of the sensor output $\bullet$, and $n_{b\bullet}$ is the fictitious noise for the bias $b_\bullet$, as shown in (35). $n_{a\ell}$ and $n_{v\ell}$ are the measurement noises of the load side acceleration, $\ddot{\theta}_\ell$, and the load side velocity, $\dot{\theta}_\ell$, respectively. $n_{\ell f}$ is the fictitious noise of the filtered load
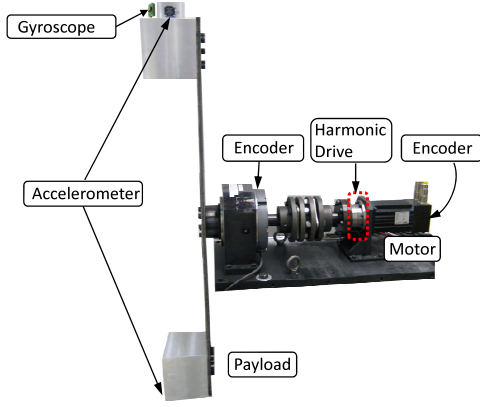
Fig. 4. Single-joint indirect drive testbed (the harmonic drive introduces friction and a mismatch between the positions of the motor and the payload).

Fig. 5. Static friction identification result (equivalent load side velocity range: −0.5 to 0.5 rad/s.)

side position, $\theta_{\ell f}$, and I_n is an $n \times n$ identity matrix. By the approximation in (39), $1/N\theta_{mf,s} = 1/NG_f(s)\theta_{m,s}(s)$ can be used as the fictitious measurement for the model output $\theta_{\ell f,s}$.

C. Kalman Filtering

The discrete time form of the extended system model (40) can be obtained by the zero-order-hold (ZOH) method. The standard Kalman filter can be formulated based on this discrete time model to estimate the load side position.

Remark 9: The KKF has several advantages compared with the dynamic model-based Kalman filter [30]. First, system representation using kinematic model is simpler than the one using dynamic model. Second, the kinematic model is an exact representation of the system states. It involves neither dynamic parameters nor external disturbances. Thus no model uncertainties need to be considered in the KKF.

Remark 10: In the proposed Kalman filter, the bias noises (n_{ba} and n_{bv}) and the output $\theta_{\ell f,s}$, are fictitious. Thus, their covariances cannot be physically identified. These fictitious noise covariances could be the design parameters for tuning the Kalman filter. Alternatively, to better handle the uncertainties in these covariances, the adaptive approach developed in [25], which uses the residual information to estimate the noise covariances, can be applied here.

V. EXPERIMENTAL RESULT

A. Experimental Setup

The proposed friction compensation method is applied to a single-joint indirect drive testbed shown in Fig. 4. The experimental setup consists of: 1) a servo motor with a 20 000 counts/revolution encoder; 2) a harmonic drive with a 80:1 gear ratio; 3) a load-side 144 000 counts/revolution encoder; and 4) a payload. The antiresonant and resonant frequencies of the setup are about 11 and 19 Hz. A MEMS gyroscope (Analog Device, Type: ADXRS150) is installed at one end of the payload and two accelerometers (Kistler, Type: 8330A3) are installed at the ends of the payload symmetrically as shown in Fig. 4. The load side encoder is only for performance evaluation. Also, the accelerometers and gyroscope are only for load side position estimation rather than direct control use, for example, $\ddot{\theta}_{\ell d}$ is used in (10) (one relaxation of Theorem 1).
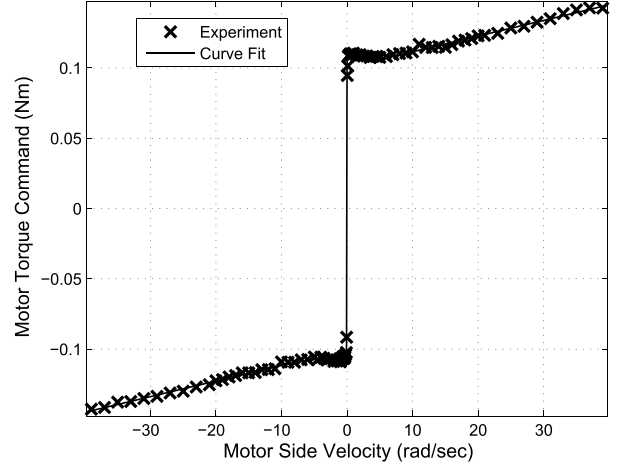
It is shown in the experiments that this does not practically influence the stability. Finally, the controller is implemented in a LabVIEW real-time target installed with LabVIEW real-time and FPGA modules. The sampling rate is selected as 1 kHz.

B. Friction Identification

Friction identification is conducted to set initial values in the adaptive friction observer. The friction regime of gross motion between surfaces is characterized by $\dot{z} = 0$, $\ddot{\theta}_m = 0$, and $\ddot{\theta}_\ell = 0$ [7]. Thus, the model in (1)–(6) is reduced to

$$u = F(\dot{\theta}_m) = \left[F_c + (F_s - F_c)e^{(-\dot{\theta}_m^2/v_s^2)}\right]\text{sgn}(\dot{\theta}_m) + \sigma_2\dot{\theta}_m. \tag{41}$$

This nonlinear function properly describes a static velocity-torque (friction force) characteristic, as shown in Fig. 5.

Each point in Fig. 5 is obtained by keeping the motor side velocity constant for the same amount of distance in a closed-loop manner. The average value of the steady-state torque (friction force $F(\dot{\theta}_m)$) at the corresponding velocity is recorded. The experiment is repeated at various velocities for the same path to obtain the whole static velocity-torque map. The nonlinear least squares method in the Optimization Toolbox of MATLAB is applied to obtain the static friction parameters, F_C, F_S, v_s, and σ_2. As shown in Fig. 5, the static friction model with these identified parameters closely captures the static friction map, including the exponential shape of the Stribeck effect.

It is shown in [7] that the dynamic parameters, σ_0 and σ_1, can be identified using an ARX (AutoRegressive with eXogenous input signal) or a BJ (Box Jenkins) model structure with presliding motion data. The resolution of the motor encoder, however, limits the implementation of this method. Thus, the method in [8] is employed here to obtain the rough estimate of σ_0, which gives $\hat{\sigma}_0 = 33.34\,\text{Nm} \cdot \text{rad}^{-1}$ when using ramp input response data, and $\hat{\sigma}_0 = 57.03\,\text{Nm} \cdot \text{rad}^{-1}$ for step input response data, respectively. Note that, the identification of σ_1 is still not available owing to the lack of a high-resolution encoder. Thus, for simplicity, it is set that $\hat{\sigma}_0 = 40\,\text{Nm} \cdot \text{rad}^{-1}$

TABLE I
IDENTIFIED FRICTION PARAMETERS (SI UNITS)

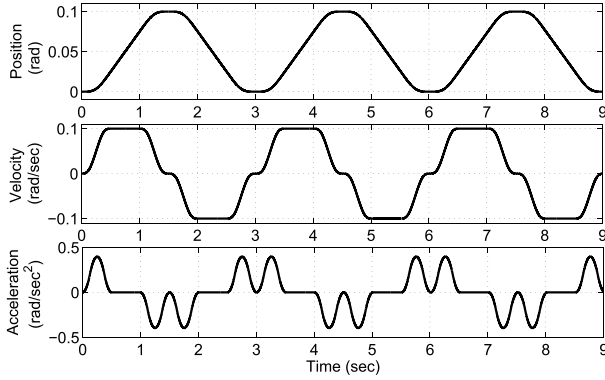| $\hat{F}_c$	$\hat{F}_s$	$\hat{v}_s$	$\hat{\sigma}_0$	$\hat{\sigma}_1$	$\hat{\sigma}_2$
0.1004	0.1075	3.951	40	0	0.001114

Fig. 6. Desired load side trajectory.

and $\hat{\sigma}_1 = 0$ Nm $\cdot$ rad^{-1} $\cdot$ s. All the identified parameters are listed in Table I.

C. Motor Side Friction Compensation

Fig. 6 shows the desired load side trajectory in this experiment, which is designed as a fourth-order time optimal trajectory suggested in [31].

1) Feedback Friction Compensation: To show the effectiveness of proposed adaptive algorithm, the estimates of friction parameters were initialized to half of the identified values. The feedback controller gains are set as $k_p = 30$, $k_v = 0.3$, and $k_i = 1.0$ (one relaxation of Theorem 1). The adaptation gains in the feedback adaptive friction compensator (*FB-A*) are selected as $[\gamma_0, \gamma_1, \gamma_2, \gamma_3, \gamma_4] = [0.001, 50\,000, 0, 0.01, 0.001]$.[4] For comparison, a feedforward Coulomb friction compensator (*FF-C*) is designed, that is, $\hat{F} = \hat{F}_c \text{sgn}(\dot{\theta}_{md})$, using the same initial guess, $\hat{F}_C$.

Fig. 7 shows the motor side and the load side tracking performance of these compensators. It is clearly seen that, motor side tracking performance is significantly improved by the *FB-A* method, converging to a suboptimal stage in about three executions. The load side performance is slightly improved with reduced peak error. Let $\|\tilde{\Theta}_\ell\|_2$, $\|\tilde{\Theta}_\ell\|_\infty$, $\|\tilde{\Theta}_m\|_2$, and $\|\tilde{\Theta}_m\|_\infty$ denote the two-norms and ∞-norms of the load side and the motor side position errors in the last repeated execution, respectively. Table II shows the performance indices improved by these algorithms compared to the case without compensation (*No-Comp.*)

Fig. 8 shows the friction estimates by *FB-A*, where $\hat{F}$ is fully adapted in about three executions. Fig. 9 shows the friction parameter adaptation process. Note that, the converged values

---

[4]The lack of a high resolution encoder limits the identification and adaptation for $\beta_0\sigma_1$. Thus, this adaptation is turned off with $\gamma_2 = 0$. This, however, does not indicate the friction dynamics is not important here. Note that, we actually only disable the adaptation of $k_2 = \beta_0\sigma_1$, while the partial effect of σ_1 is still included into the adaptation of $k_0 = \sigma_1 + \sigma_2$. Therefore, the friction dynamics is (partially) addressed and compensated in this case, where the testing trajectory is low speed and has several velocity reversal periods for checking the dynamic transient response.
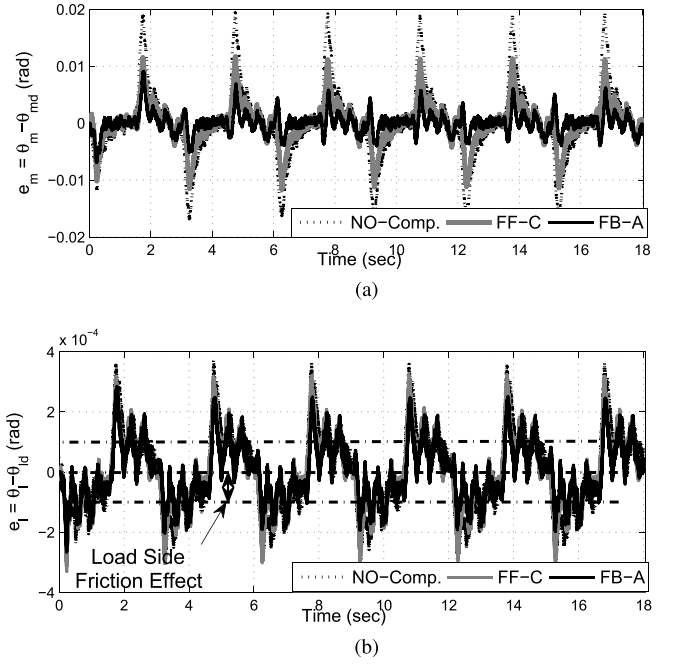

(a)

(b)

Fig. 7. Performance of the motor side compensators. (a) Motor side position tracking error. (b) Load side position tracking error. (*No-Comp.* [black-dot]: without friction compensator; *FF-C* [gray-solid]: feedforward Coulomb friction compensator; *FB-A* [black-solid]: feedback adaptive friction compensator at motor side only.)

TABLE II
IMPROVEMENTS COMPARED WITH THE *No-Comp.* CASE

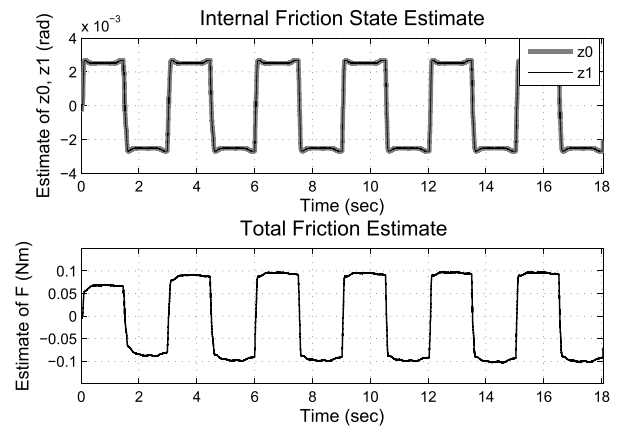|	*FF-C*	*FB-A*	*FF-A*	*Hybrid*
$\|\tilde{\Theta}_\ell\|_2$	18.30%	35.26%	37.61%	66.05%
$\|\tilde{\Theta}_\ell\|_\infty$	12.69%	32.81%	35.23%	65.77%
$\|\tilde{\Theta}_m\|_2$	45.66%	74.41%	78.53%	75.74%
$\|\tilde{\Theta}_m\|_\infty$	41.74%	68.30%	73.31%	74.78%

Fig. 8. Friction estimates by *FB-A* observer.

are not exactly twice the initial values. This is first because the identified nominal values may not be exactly the actual values. Secondly, as discussed in Theorem 1, the motor side friction compensation aims at reducing the motor side tracking error rather than accurate parameter estimation, especially for the non-persistently exciting trajectory used here. Also the friction
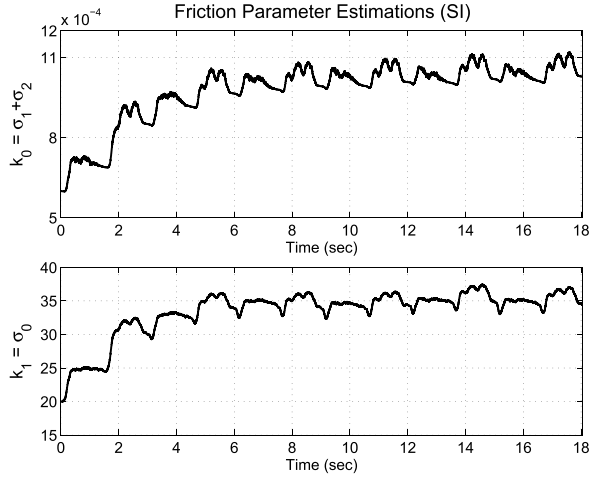
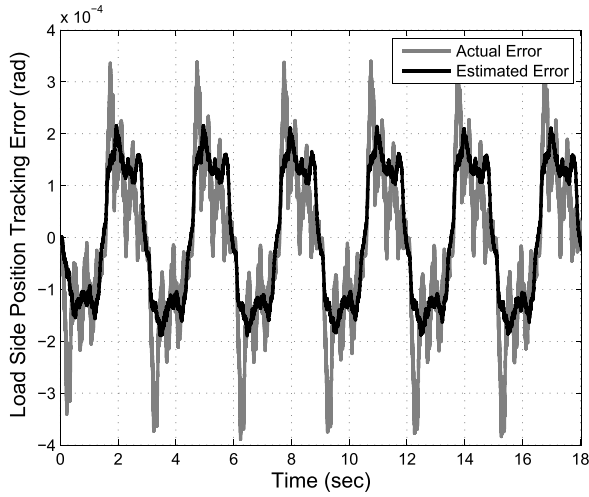Fig. 9.   Friction parameter estimations.

Fig. 10.   Load side actual and estimated position tracking error.
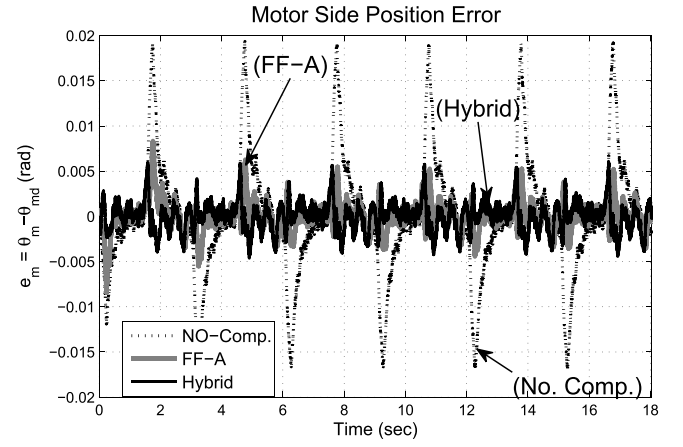

Fig. 11.   Performance of the hybrid compensator. (a) Motor side position tracking error. (b) Load side position tracking error. (*No-Comp.* [black-dot]: without friction compensator; *FF-A* [gray-solid]: feedforward adaptive friction compensator at motor side only; *Hybrid* [black-solid]: hybrid compensator at the state q_1.)

model structure is modified to adapt only three parameters. Besides, $\hat{k}_2$ is kept zero since $\hat{\sigma}_1 = 0$ and $\gamma_2 = 0$.

2) Feedforward Friction Compensation: The modification of the proposed adaptive friction observer from the feedback form to the feedforward form is also applied in the experiment. The same controller gains, k_p, k_v, and k_i, and adaptation gains, γ_0, γ_1, and γ_2, from *FB-A*, are used in the feedforward compensator (*FF-A*). Table II shows that *FF-A* slightly improves the performance of *FB-A*.
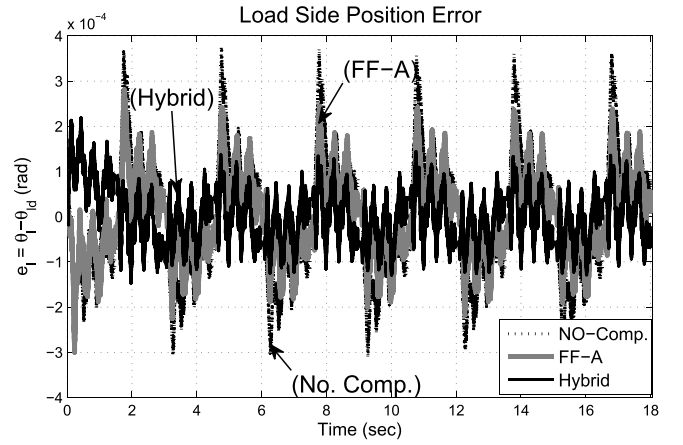
The motor side compensation result (e.g., Fig. 7) shows that, even if the motor side performance is significantly improved, little improvement can be observed at the load side. In Fig. 7, the oscillation in the load side position tracking error is mainly due to the transmission error [32], while the offset in the tracking error is due to the load side friction effects explained by (11). This indicates the necessity to implement the load side friction compensation.

D. Load Side Position Estimation

To implement the load side friction compensation, the load side position estimation method (i.e., KKF) needs to be applied first.

Fig. 10 shows the actual and the estimated tracking errors of the load side position in the *No-Comp.* experiment. It shows that the tracking error estimated by KKF captures most trends (especially the offset) of the actual tracking error.[5] Therefore, KKF can provide effective load side position estimation for the load side friction compensation scheme.

E. Load Side Friction Compensation

Now the load side friction compensation is enabled with the proposed hybrid scheme. To show the effectiveness of the proposed load side compensation algorithm, $\hat{r}_\ell$ was initialized to $1.0N$ where N is the reducer gear ratio. Fig. 11 shows the performance of friction compensator enabled on both the motor side and the load side (*Hybrid*), that is, the state q_1 in Fig. 3. It shows that the load side position tracking error offset is significantly reduced[6] by the hybrid compensator scheme (*Hybrid*) in less than one execution, while the motor side

---

[5]The minor oscillatory error not estimated by KKF is mainly due to the transmission error effect which is not considered in the estimation algorithm.

[6]The transient performance is also significantly improved at the velocity reversals, where the load side friction modeling may not be strictly valid.
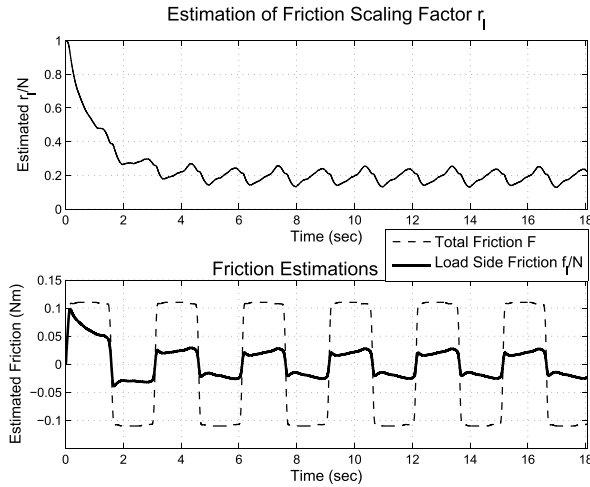
Fig. 12.   Load side friction estimates.

tracking performance is maintained at about the same level. This is also confirmed by the performance indices in Table II. The convergence of the estimated friction ratio $\hat{r}_\ell$ and the estimated load side friction $\hat{f}_\ell$ is shown in Fig. 12.

VI. CONCLUSION

To improve the load side tracking performance, we have investigated the friction compensation in indirect drive mechanisms by separating the problem into two parts, that is, motor side and load side. The motor side compensator employed the idea of torque compensation using an adaptive friction observer based on the modified LuGre model, while the load side compensator was implemented by injecting the load side friction estimate into the generated motor side reference. A hybrid compensator scheme was proposed to engage or disengage the load side compensator. Because of the lack of load side position measurement, a sensor fusion scheme was also developed to provide the essential load side position estimate. It has been shown that additional care should be placed to the load side friction in addition to the friction effects on the motor side. Experimental results demonstrated the effectiveness of the proposed scheme to achieve the ultimate objective of enhancing load side performance.

Note that the proposed method was still focused on a single-joint indirect drive mechanism. For the extension to the indirect drive train with multiple joints (such as the multi-joint robot manipulator), the robot dynamic and kinematic models will be needed to decouple the problem into the joint level to apply the proposed method for friction compensation. Motivated by this, we have developed a joint state estimation algorithm in [33] and decoupled the control problem into the joint level for dual-stage iterative learning control in [34]. However, the real-time application of the proposed friction compensation method to the multi-joint robot is still among our future work.

REFERENCES

[1] M. W. Spong, "Modeling and control of elastic joint robots," *J. Dyn. Syst. Meas. Control*, vol. 109, no. 4, pp. 310–319, 1987.

[2] M. Ruderman, F. Hoffmann, and T. Bertram, "Modeling and identification of elastic robot joints with hysteresis and backlash," *IEEE Trans. Ind. Electron.*, vol. 56, no. 10, pp. 3840–3847, Oct. 2009.

[3] M. Ruderman, "Modeling of elastic robot joints with nonlinear damping and hysteresis," in *Robotic Systems—Applications, Control and Programming*. Rijeka, Croatia: InTech, 2012, pp. 293–312.

[4] B. Armstrong-Hélouvry, P. Dupont, and C. C. De Wit, "A survey of models, analysis tools and compensation methods for the control of machines with friction," *Automatica*, vol. 30, no. 7, pp. 1083–1138, 1994.

[5] C. C. De Wit, H. Olsson, K. J. Astrom, and P. Lischinsky, "A new model for control of systems with friction," *IEEE Trans. Autom. Control*, vol. 40, no. 3, pp. 419–425, Mar. 1995.

[6] M. Tomizuka, "On the compensation of friction forces in precision motion control," in *Proc. Asia-Pacific Workshop Adv. Motion Control*, Jul. 1993, pp. 69–74.

[7] F. Altpeter, "Friction modeling, identification and compensation," Ph.D. dissertation, Dept. Comput. Commun. Sci., École Polytechnique Fédérale de Lausanne, Lausanne, Switzerland, 1999.

[8] C. Canudas de Wit and P. Lischinsky, "Adaptive friction compensation with partially known dynamic friction model," *Int. J. Adapt. Control Signal Process.*, vol. 11, no. 1, pp. 65–80, 1997.

[9] L. Xu and B. Yao, "Adaptive robust control of mechanical systems with nonlinear dynamic friction compensation," in *Proc. Amer. Control Conf.*, vol. 4. 2000, pp. 2595–2599.

[10] K. Ohnishi, "A new servo method in mechatronics," *Trans. Jpn. Soc. Electr. Eng.*, vol. 107-D, no. 1, pp. 83–86, 1987.

[11] M. Tomizuka, T.-C. Tsao, and K. Chew, "Discrete-time domain analysis and synthesis of repetitive controllers," *ASME J. Dyn. Syst., Meas., Control*, vol. 111, no. 3, pp. 353–358, 1989.

[12] E. D. Tung, G. Anwar, and M. Tomizuka, "Low velocity friction compensation and feedforward solution based on repetitive control," *J. Dyn. Syst. Meas. Control*, vol. 115, no. 2A, pp. 279–284, 1993.

[13] H. D. Taghirad and P. R. Belanger, "Modeling and parameter identification of harmonic drive systems," *J. Dyn. Syst. Meas. Control*, vol. 120, no. 4, pp. 439–444, 1998.

[14] P. S. Gandhi, F. H. Ghorbel, and J. Dabney, "Modeling, identification, and compensation of friction in harmonic drives," in *Proc. 41st IEEE Conf. Decision Control*, vol. 1. Dec. 2002, pp. 160–166.

[15] S. Jeon and M. Tomizuka, "Limit cycles due to friction forces in flexible joint mechanisms," in *Proc. IEEE/ASME Int. Conf. Adv. Intell. Mechatron.*, Jul. 2005, pp. 723–728.

[16] R. Dhaouadi, "Nonlinear friction compensation in harmonic drives with hysteresis," in *Proc. IEEE/ASME Int. Conf. Adv. Intell. Mechatron.*, vol. 1. Jul. 2003, pp. 278–283.

[17] J. P. Hauschild, G. Heppler, and J. McPhee, "Friction compensation of harmonic drive actuators," in *Proc. 6th Int. Conf. Dyn. Control Syst. Struct. Space*, Liguria, Italy, Jul. 2004, pp. 683–692.

[18] N. Mallon, N. van de Wouw, D. Putra, and H. Nijmeijer, "Friction compensation in a controlled one-link robot using a reduced-order observer," *IEEE Trans. Control Syst. Technol.*, vol. 14, no. 2, pp. 374–383, Mar. 2006.

[19] H. D. Teghirad and P. R. Belanger, "Robust friction compensator for harmonic drive transmission," in *Proc. IEEE Int. Conf. Control Appl.*, vol. 1. Sep. 1998, pp. 547–551.

[20] H. Salmasi, R. Fotouhi, and P. N. Nikiforuk, "On the stability of a friction compensation strategy for flexible-joint manipulators," *Adv. Robot.*, vol. 24, no. 15, pp. 2059–2086, 2010.

[21] Z. Wen-Hong and M. Doyon, "Adaptive control of harmonic drives," in *Proc. 43rd IEEE Conf. Decision Control*, vol. 3. Dec. 2004, pp. 2602–2608.

[22] T. Tjahjowidodo, F. Al-Bender, H. Van Brussel, and W. Symens, "Positioning controller for mechanical systems with a mini harmonic drive servo actuator," in *Proc. IEEE/ASME Int. Conf. Adv. Intell. Mechatron.*, Sep. 2007, pp. 1–6.

[23] W. Chen, K. Kong, and M. Tomizuka, "Hybrid adaptive friction compensation of indirect drive trains," in *Proc. ASME Dyn. Syst. Control Conf.*, Oct. 2009, pp. 313–320.

[24] P. Roan, N. Deshpande, Y. Wang, and B. Pitzer, "Manipulator state estimation with low cost accelerometers and gyroscopes," in *Proc. IEEE/RSJ Int. Conf. Intell. Robot. Syst.*, Oct. 2012, pp. 4822–4827.

[25] W. Chen and M. Tomizuka, "Estimation of load side position in indirect drive robots by sensor fusion and Kalman filtering," in *Proc. Amer. Control Conf.*, Jun./Jul. 2010, pp. 6852–6857.

[26] Y. Tan and I. Kanellakopoulos, "Adaptive nonlinear friction compensation with parametric uncertainties," in *Proc. Amer. Control Conf.*, vol. 4. 1999, pp. 2511–2515.

[27] J.-J. E. Slotine and W. Li, *Applied Nonlinear Control*. Upper Saddle River, NJ, USA: Prentice-Hall, 1991.

[28] Y. D. Landau, *Adaptive Control: The Model Reference Approach*. London, U.K.: IET, 1979.

[29] D. J. Lee and M. Tomizuka, "State/parameter/disturbance estimation with an accelerometer in precision motion control of a linear motor," in *Proc. ASME IMECE*, New York, Nov. 2001, pp. 11–16.

[30] S. Jeon and M. Tomizuka, "Benefits of acceleration measurement in velocity estimation and motion control," *Control Eng. Pract.*, vol. 15, no. 3, pp. 325–332, Mar. 2007.

[31] P. Lambrechts, M. Boerlage, and M. Steinbuch, "Trajectory planning and feedforward design for electromechanical motion systems," *Control Eng. Pract.*, vol. 13, no. 2, pp. 145–157, 2005.

[32] C.-H. Han, C.-C. Wang, and M. Tomizuka, "Suppression of vibration due to transmission error of harmonic drives using peak filter with acceleration feedback," in *Proc. 10th IEEE Int. Workshop Adv. Motion Control*, Mar. 2008, pp. 182–187.

[33] W. Chen and M. Tomizuka, "Load side state estimation in elastic robots with end-effector sensing," in *Proc. IEEE/ASME Int. Conf. AIM*, Kaohsiung, China, Jul. 2012, pp. 598–603.

[34] W. Chen and M. Tomizuka, "Iterative learning control with sensor fusion for robots with mismatched dynamics and mismatched sensing," in *Proc. ASME Dyn. Syst. Control Conf.*, Fort Lauderdale, FL, USA, Oct. 2012, pp. 1480–1488.

Wenjie Chen (S'12–M'12) received the B.Eng. degree in mechanical engineering from Zhejiang University, Zhejiang, China, in 2007, and the M.S. and Ph.D. degrees in mechanical engineering from the University of California at Berkeley, Berkeley, CA, USA, in 2009 and 2012, respectively.

He was a Post-Doctoral Scholar with the Department of Mechanical Engineering, University of California at Berkeley. He joined the Robot Laboratory, FANUC Corporation, Oshino-mura, Japan, as a Senior Development Engineer for Learning Robot Development, in 2013. His current research interests include design and implementation of advanced control, sensing, and learning algorithms with applications to robotic/mechatronic systems, such as industrial robots, wearable assistive robotics, and robots for advanced manufacturing.

Kyoungchul Kong (S'04–M'09) received the B.Eng. (*summa cum laude*) degree in mechanical engineering, the B.S. degree in physics in 2004, the M.S. degree in mechanical engineering from Sogang University, Seoul, Korea, in 2006, and the Ph.D. degree in mechanical engineering from the University of California at Berkeley, Berkeley, CA, USA, in 2009.

He was a Post-Doctoral Research Fellow with the Department of Mechanical Engineering, University of California at Berkeley. He joined the Department of Mechanical Engineering, Sogang University, Seoul, Korea, as an Assistant Professor, in 2011. He has been involved in researches on control systems and mechatronics. His current research interests include design, modeling, and control of mechatronic systems with emphasis on locomotion and mobility of human-centered robotic systems.

Masayoshi Tomizuka (M'86–F'97) received the Ph.D. degree in mechanical engineering from the Massachusetts Institute of Technology, Cambridge, MA, USA, in 1974.

He joined the Department of Mechanical Engineering, University of California at Berkeley, Berkeley, CA, USA, in 1974, where he is currently the Cheryl and John Neerhout, Jr., Distinguished Professor. He has been involved in researches on optimal and adaptive control, digital control, motion control, and their applications to robotics, manufacturing, information storage devices, and vehicles. He served as the Program Director of the Dynamic Systems and Control Program with the National Science Foundation from 2002 to 2004.

Dr. Tomizuka was the Technical Editor of the *ASME Journal of Dynamic Systems, Measurement and Control* and the Editor-in-Chief of the IEEE/ASME TRANSACTIONS ON MECHATRONICS. He was the recipient of the Rudolf Kalman Best Paper Award from the American Society of Mechanical Engineers (ASME) in 1995 and 2010, the Charles Russ Richards Memorial Award from ASME in 1997, the Rufus Oldenburger Medal from ASME in 2002, and the John R. Ragazzini Award from the American Automatic Control Council in 2006.